Clim Dyn (2014) 43:753–770
DOI 10.1007/s00382-013-1817-6

A synoptic and dynamical characterization of wave-train and blocking cold surge over East Asia

Tae-Won Park · Chang-Hoi Ho · Yi Deng

Received: 1 April 2013 / Accepted: 24 May 2013 / Published online: 4 June 2013

Abstract Through an agglomerative hierarchical clustering method, cold surges over East Asia are classified into two distinct types based on the spatial pattern of the geopotential height anomalies at 300 hPa. One is the wave-train type that is associated with developing large-scale waves across the Eurasian continent. The other is the blocking type whose occurrence accompanies subarctic blocking. During the wave-train cold surge, growing baroclinic waves induce a southeastward expansion of the Siberian High and strong northerly winds over East Asia. Blocking cold surge, on the other hand, is associated with a southward expansion of the Siberian High and northeasterly winds inherent to a height dipole consisting of the subarctic blocking and the East Asian coastal trough. The blocking cold surge tends to be more intense and last longer compared to the wave-train type. The wave-train cold surge is associated with the formation of a negative upper tropospheric height anomaly southeast of Greenland approximately 12 days before the surge occurrence. Further analysis of isentropic potential vorticity reveals that this height anomaly could originate from the lower stratosphere over the North Atlantic. Cold surge of the blocking type occurs with an amplifying positive geopotential and a negative potential vorticity anomaly over the Arctic and the northern Eurasia in stratosphere. These anomalies resemble the stratospheric signature of a negative phase of the Arctic Oscillation. This stratospheric feature is further demonstrated by the observation that the blocking type cold surge occurs more often when the Arctic Oscillation is in its negative phase.

T.-W. Park (✉) · Y. Deng
School of Earth and Atmospheric Sciences,
Georgia Institute of Technology, Atlanta, GA, USA
e-mail: park2760@gmail.com; taewon.park@eas.gatech.edu

C.-H. Ho
School of Earth and Environmental Sciences,
Seoul National University, Seoul, South Korea

1 Introduction

Accompanied by an abrupt enhancement of the Siberian High, a semi-permanent low-level pressure system with no marked upper-level pressure ridge observed, cold surges lead to rapid temperature drops exceeding the intra-winter variability of temperature (i.e., a specific standard deviation) within one or 2 days. Sustained for several days with intense northerly winds, cold surges exert tremendous socioeconomic impacts on East Asian countries. On average, there are about ten cold surges over East Asia every winter (Chen et al. 2004). They bring heavy freezing precipitation including snowfall into East Asia (Chen 2002; Jeong et al. 2008; Park et al. 2010). Strong cold surge events often cause anomalous convective activity over the South China Sea and adjacent regions (Chen et al. 2002), and sometimes even leads to anomalous atmospheric circulation (e.g., geopotential height and wind fields), surface temperature, and precipitation in remote areas such as North America (Cohen et al. 2001; Yang et al. 2002).

The Siberian High is built and maintained by a heat sink related to strong radiative cooling and a heat source due to large-scale descending motion (Ding and Krishnamurti 1987). The amplification of the Siberian High and its expansion into East Asia is well known as an essential factor for the generation and maintenance of cold surges (Zhang et al. 1997; Gong and Ho 2002; Takaya and Nakamura 2005a). With a prevailing northwesterly wind over the southern Siberia, the sudden expansion of the high pressure and the corresponding intense cold air advection

induce severe cold surges affecting nearly the entire East Asian region. Previous studies have investigated East Asian cold surges and the related upper-tropospheric wave-train across the Eurasian Continent responsible for cold surge occurrences (Jeong et al. 2006; Lau and Lau 1984; Zhang et al. 1997). In particular, Takaya and Nakamura (2005a) have suggested an important role of intraseasonal amplification of the Siberian High on the link between the wave-train and the occurrence of cold surges. The southeastward propagation of the wave-train deepens the East Asian coastal trough, leading to a lower-level northwesterly flow that induces an advection of the preexisting cold anomalies over Siberia (Zhang et al. 1997; Joung and Hitchman 1982). The anomalous anticyclonic circulation accompanying the cold anomaly is a direct indicator of the expansion of the Siberian High and in turn, induce anomalous vorticity advection aloft that reinforces the blocking ridge and cyclonic anomalies downstream of it that constitute the propagation wave-train. The interaction among the wave-train, the Siberian High, and the preexisting cold anomalies over Siberia thus plays a critical role in triggering and sustaining cold surges over East Asia (Takaya and Nakamura 2005a).

In addition to the initiation of cold surges by Rossby wave-trains, atmospheric blocking is a second way in which cold surges can be produced. Based on composite analysis applied to the 20 strongest Siberian Highs, Takaya and Nakamura (2005b) showed that the amplification of the Siberian High and the subsequent cold surge could have two different origins—a wave-train across the Eurasian Continent emanated from the North Atlantic and a blocking anticyclone moving westward from the North Pacific. Based on a case study of an extremely cold winter (2005/2006), Park et al. (2008) reported two distinct patterns of amplification of the Siberian High that result in cold surge occurrences: a growing baroclinic wave across Eurasia and a high-latitude blocking slowly retrogressed from the Arctic region. Park et al. (2011) further showed that the blocking type tends to occur during the negative Arctic Oscillation (AO) phase (e.g., Thompson and Wallace 1998), while the wave-train type is observed during both positive and negative AO phases.

Although aforementioned studies introduced two types of amplification of the Siberian High and the related cold surges, the lifecycle and dynamical characterization of these two types of cold surge have not been fully investigated. No attempts have been made to objectively classify East Asian cold surge events using the recent and complete observational record. This study aims to address these issues by first grouping observed cold surges into the wave-train and the blocking type through cluster analysis then documenting the lifecycle characteristics and dynamical precursors before the occurrences of these two types of surges.

This paper is organized as follows. Section 2 gives a brief description of the data used, cold surge definition, and the cluster analysis method adopted to group the cold surges into two types. The distinct features of the wave-train and the blocking cold surge are described in Sect. 3, followed by a discussion of respective dynamical signals prior to both types of cold surges in Sect. 4. Section 5 summarizes the findings of this study and discusses their implications for winter weather prediction and climate projections over East Asia.

2 Data and methodology

2.1 Data

To identify cold surge events over East Asia, we use daily mean surface air temperature (SAT) from 103 stations in China and 13 stations in Korea (see Fig. 1), and daily mean Sea Level Pressure (SLP) from the National Centers for Environmental Prediction–National Center for Atmospheric Research (NCEP–NCAR) reanalysis (Kalnay et al. 1996), which has a horizontal resolution of 2.5° longitude by 2.5° latitude and 17 pressure levels in the vertical ranging from 1,000 to 10 hPa. In addition, pressure-level data from the NCEP–NCAR reanalysis, including daily mean temperature (T), geopotential height (Z), and zonal and meridional winds, are analyzed to provide a synoptic and dynamical characterization of cold surges. The present study mainly uses the daily anomalies with respect to a daily annual cycle at each station or grid-point.

The monthly mean AO index used in the present study is obtained from the National Oceanic and Atmospheric Administration (NOAA) Climate Prediction Center (CPC) (ftp://ftp.cpc.ncep.noaa.gov/cwlinks/). The analysis conducted here is restricted to the Northern Hemisphere cool season (November–March) when the East Asian winter monsoon dominates and cold surge activity peaks. Considering the availability and reliability of data, especially SAT, we focus on 52 cool-seasons in the period 1954/1955–2005/2006.

2.2 Definition of cold surge

An expansion of the Siberian High and the subsequent steep drop of SAT within 1 or 2 days are essential features of a cold surge over East Asia. To capture both features, previous studies have employed various synoptic criteria such as the strong Siberian High (e.g., $\geq$1,035 hPa) and a specific fixed temperature drop (e.g., $\geq$9 °C) (Chen et al. 2004; Zhang et al. 1997) or a specific region-dependent temperature drop (e.g., $\geq$the intra-winter variability over the given region) (Jeong and Ho 2005; Park et al. 2011).

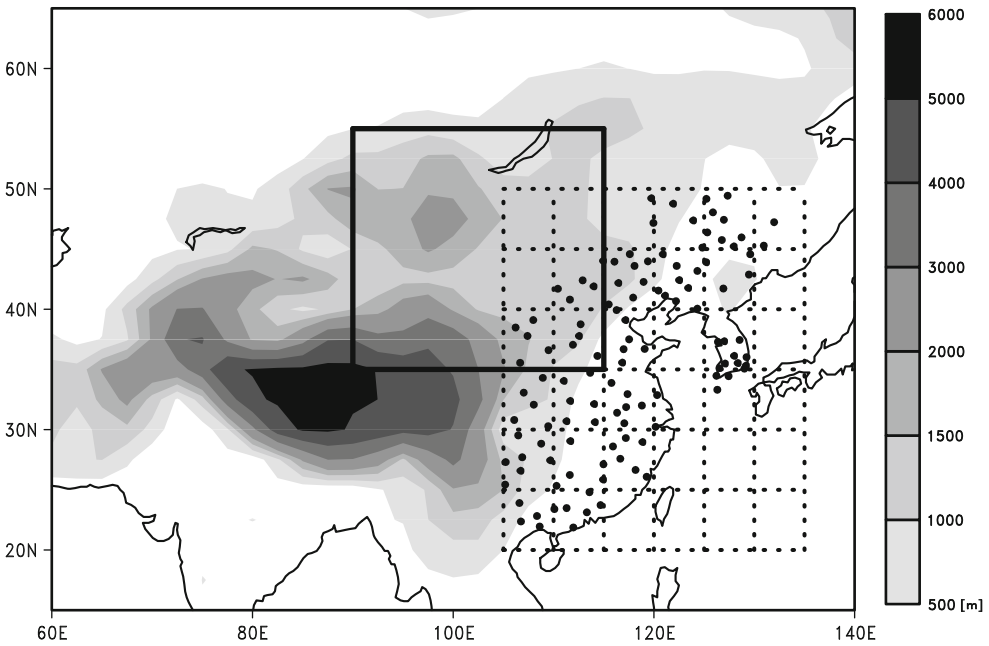

Fig. 1 Distribution of 116 observation stations over East Asia (*closed circles*), 5° × 5° grid *boxes* (*dotted lines*), and the Siberian high domain (*thick solid lines*). *Shadings* indicate the topography

Here we follow the methodology of Park et al. (2011). In the first step, we identify days of the strong Siberian High expansion as those when the magnitudes of the SLP and relative vorticity at the center of the surface anticyclone over 90°E–115°E, 35°N–55°N (Fig. 1) exceed 1,035 hPa and -1.0×10^{-5} s^{-1}, respectively. The center of the surface anticyclone is defined as the grid point where the Z at 1,000 hPa is larger than the values of the eight surrounding grid points (Zhang and Wang 1997). In the second step, days of abrupt SAT drop are identified. Since our focus is on synoptic-scale cold surges that are accompanied by upper-level circulation anomalies, smaller-scale anomalous cold temperature due to local effect such as radiative cooling must be excluded. To achieve this, we cast the 116 East Asian stations into 5° × 5° grid boxes, and calculate the SAT values averaged over these boxes (Fig. 1). When SLP criterion must be met, a cold surge day is defined as a day when the drop of the averaged SAT ($SAT_t - SAT_{t-1}$) exceeds 1.5 σ (sigma, standard deviation of daily SAT during the 52 cool-seasons) in more than one grid box. Some early studies (Zhang et al. 1997; Jeong and Ho 2005) adopt the only day-to-day SAT drop in cold surge definition. The definition regardless of the SAT anomaly often detects cold surges with positive SAT anomalies in spite of steep SAT decreases. To remove these "warm" cold surge events from our analysis, we have added a third criterion in cold surge definition that the averaged daily SAT anomaly has to be less than −1.5 σ in order for that day to be considered a cold surge day. Given all three criteria described above, a total of 332 cold surges are detected for the period under consideration.

2.3 Clustering method

To objectively classify all cold surges into two groups—the wave-train type and the blocking type, we apply an agglomerative hierarchical clustering method to 300-hPa Z anomalies (i.e., deviation from the climatological daily mean for the years of the analysis data set) averaged over a box located between 60°E–180° and 20°N–90°N where main features of the wave-train and the blocking are observed. In this method, each individual case (i.e., a vector containing height anomalies over multiple grid point locations of the study region) is regarded as a single object and is considered as a single cluster at the first step. Then, the number of clusters decreases by one per step due to the merging of two clusters. For example, if there are 332 cases, the number of clusters at the first step is 332, and then the merging of two clusters makes it 331 clusters at the second step. Here we performed the clustering algorithm following the Ward's minimum variance clustering criterion (Kalkstein et al. 1987). Let us consider G clusters at tth step. According to this criterion, the distance within each cluster is first defined as the squared sum of the differences between individual objects within the cluster and their mean and the distance for the gth cluster is called the Error Sum of Squares (ESS_g). Then the total distance for G clusters (Total Error Sum of Squares, $TESS_G$) is defined as sum of ESS_g, where

$$TESS_G = \sum_{g=1}^{G} ESS_g = \sum_{g=1}^{G} \sum_{i=1}^{n_g} (x_i - \overline{x_g})^2 \quad (1)$$

In Eq. (1), x_i and $\overline{x_g}$ are individual objects in the gth cluster and their mean, respectively. n_g is the number of objects in the gth cluster. Now, let us consider the criterion to select a pair of clusters among the G clusters to combine in order to make the total number of clusters $G - 1$ at the (t + 1)th step. The two clusters whose combination results in the smallest increase from $TESS_G$ to $TESS_{G-1}$ (i.e., the combination is done for the two most "similar" clusters) is selected. In other words, the merging that minimizes the increase from $TESS_G$ to $TESS_{G-1}$ is the criterion to select the pair of clusters for combination. This combination process is repeated and the total distance for all clusters increases every step. After recording the increase of the $TESS_G$ (i.e., the distance) during each step until a final, single cluster is reached, we will identify the step that corresponds to the GREATEST increase of the total distance. This largest increase implies that we are merging two clusters which have the most DIFFERENT characteristics (i.e., in this study geopotential height anomaly) each other. In other words, these two clusters should not be merged. This is therefore the step when the actual merging procedure should be terminated. We will document the total number of clusters at this termination step the final number of cluster.

In the present study, the greatest increase of the total distance between clusters is occurring between 330th and 331st (i.e., the last step) steps (not shown here). It indicates that the clustering procedure should be terminated at 330th step and the final number of clusters is two. As the result of this clustering method, a total of 332 cold surge cases are classified into two groups—273 as the wave-train type and 59 as the blocking type and the composites of the daily anomalies related to the two types have been conducted. The daily anomalies are calculated based on differences from a daily annual cycle at each station or grid-point. To reveal statistical significance for the composited results of anomalies, the student t test is applied to the each type of cold surges.

The results of the present study are wholly based on the agglomerative hierarchical clustering method to classify all cold surges into the wave-train and the blocking types. There are two types of hierarchical clustering: agglomerative and divisive methods. The clustering result based on divisive method also produces two clusters and the individual cold surge cases in each cluster are nearly equal to those classified by agglomerative method. In the agglomerative hierarchical clustering method, the Ward's minimum variance clustering criterion is used to estimate the total distance between clusters. To confirm our results, we need to use various clustering criteria of the total distances obtained from mean of all objects in one cluster, cluster centroid, the furthest apart objects, the nearest objects, and so on. Applications of the other criteria classify all cold surges into the two types, though there is a little difference in the number of the cold surges to belong to the two types. Thus, it is important to point out that the results presented here are not sensitive to the specific clustering criteria employed.

2.4 Isentropic potential vorticity

The anomalies of potential vorticity (*PV*) and its isentropic value (*IPV*) prior to cold surges are also evaluated for each type of cold surge. Following the methodology of Hoskins et al. (1985), the PV on the isobaric coordinate is first calculated by using the expression

$$PV = -g(f\vec{k} + \nabla_p \times \vec{V}) \cdot \nabla_p \theta, \quad (2)$$

where ∇p is the three-dimensional gradient operator in xyp space; g, f, p, θ are the gravity constant, Coriolis parameter, pressure and potential temperature, respectively; $\vec{V}$ is the three-dimensional wind vector and $\vec{k}$ is the local unit vector in the vertical direction. Subsequently, a linear interpolation on constant θ surface yields the IPV defined as

$$IPV = -g(f + \vec{k} \cdot \nabla_\theta \times \vec{V}) \frac{\partial \theta}{\partial p}. \quad (3)$$

In Eq. (3), ∇_θ is the three-dimensional gradient operator in $xy\theta$ space.

3 Synoptic characterization of wave-train and blocking cold surge

Before showing the classified results, we investigate the upper-tropospheric Z patterns related to two types of the cold surges dealt with by previous studies. Figure 2 displays the 300-hPa Z anomalies associated with several cold surge cases that have been investigated in previous studies. Figure 2a, b correspond to two cases (21 December 1973 and 18 February 1968) analyzed by Joung and Hitchman (1982) and Fig. 2c–e are events (4 January 1980, 14 January 1982, and 4 December 1982) studied by Ding and Krishnamurti (1987). Figure 2f shows the 300-hPa Z anomalies associated with a cold surge that occurred on 19–23 December 2001 and had been simulated by Lu et al. (2007). Figure 2g, h are two events from the 2005/06 winter (4 January 2006 and 4 December 2005), both of which have been investigated by Park et al. (2008). Cold surges in Fig. 2a, c, e, and g are related to an upper-tropospheric wave-train

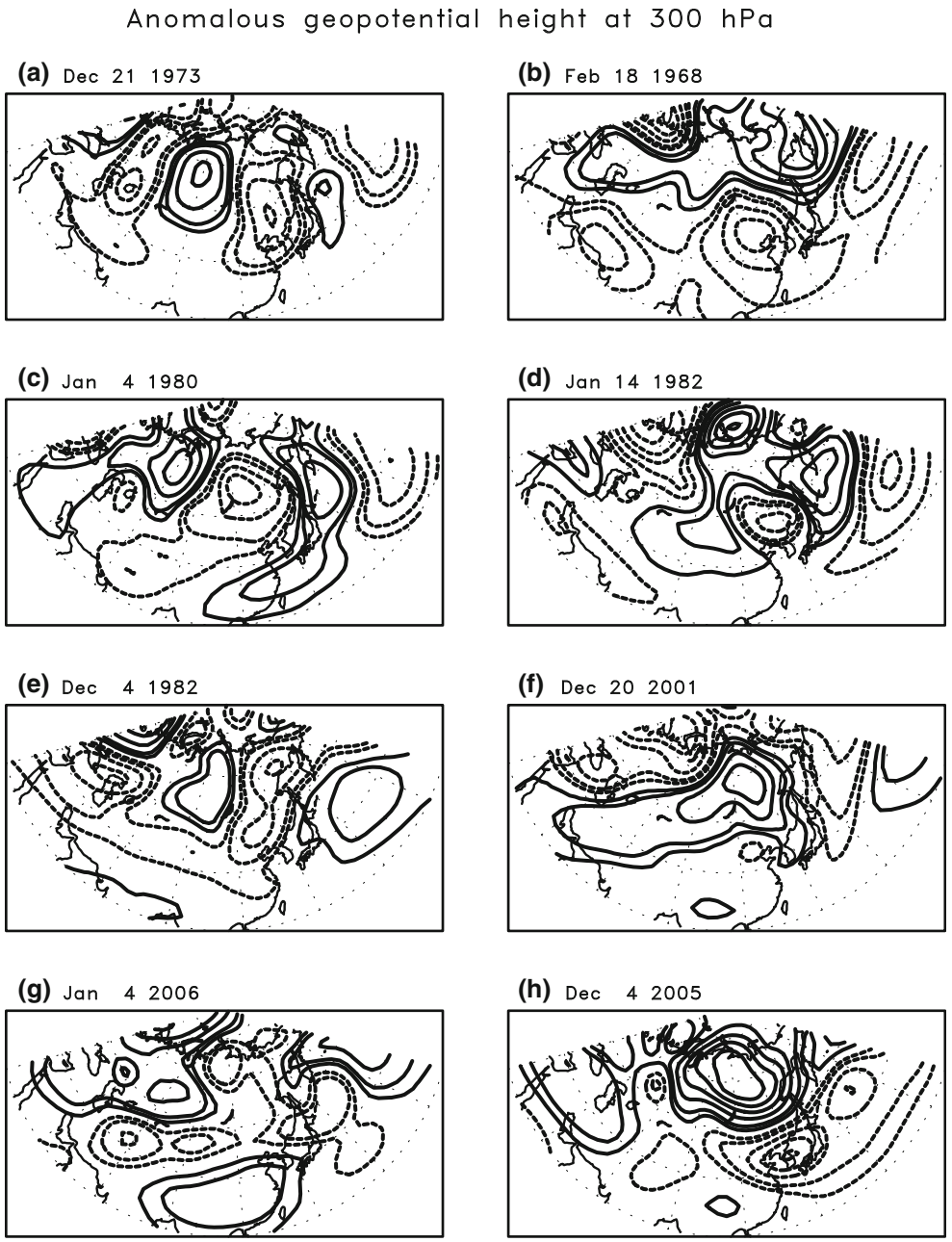

Fig. 2 300-hPa Z anomalies (contour; in intervals of 50 m, the *solid* and *dashed* contours refer to positive and negative values, respectively.) for cold surges occurred on **a** 21 December 1973, **b** 18 February 1968, **c** 4 January 1980, **d** 14 January 1982, **e** 4 December 1982, **f** 20 December 2001, **g** 4 January 2006, and **h** 4 December 2005. These cold surges are analyzed in some previous studies (Joung and Hitchman 1982; Ding and Krishnamurti 1987; Lu et al. 2007; Park et al. 2008)

originating from the interior of Eurasia. The ridge-trough-ridge pattern generally aligns in a northwest-southeast direction across East Asia, with the exception of Fig. 2g in which the wave-train is oriented in a north–south direction that aligns from the Siberia to south China. On the other hand, a dipole pattern with positive (negative) Z anomalies over the subarctic (East Asian coast) is shown in Fig. 2b, d, f, and h. This dipole structure suggests that upper-level circulation anomalies accompanying cold surges of the blocking type constitutes a high-latitude blocking and a coastal trough (Park et al. 2011). In the present study, the synoptic and dynamical features of the two types of cold surge are generalized through a composite analysis based upon the results of cluster analysis. The cold surges in left (right) column of Fig. 2 are classified into the cluster of the wave-train (blocking) type.

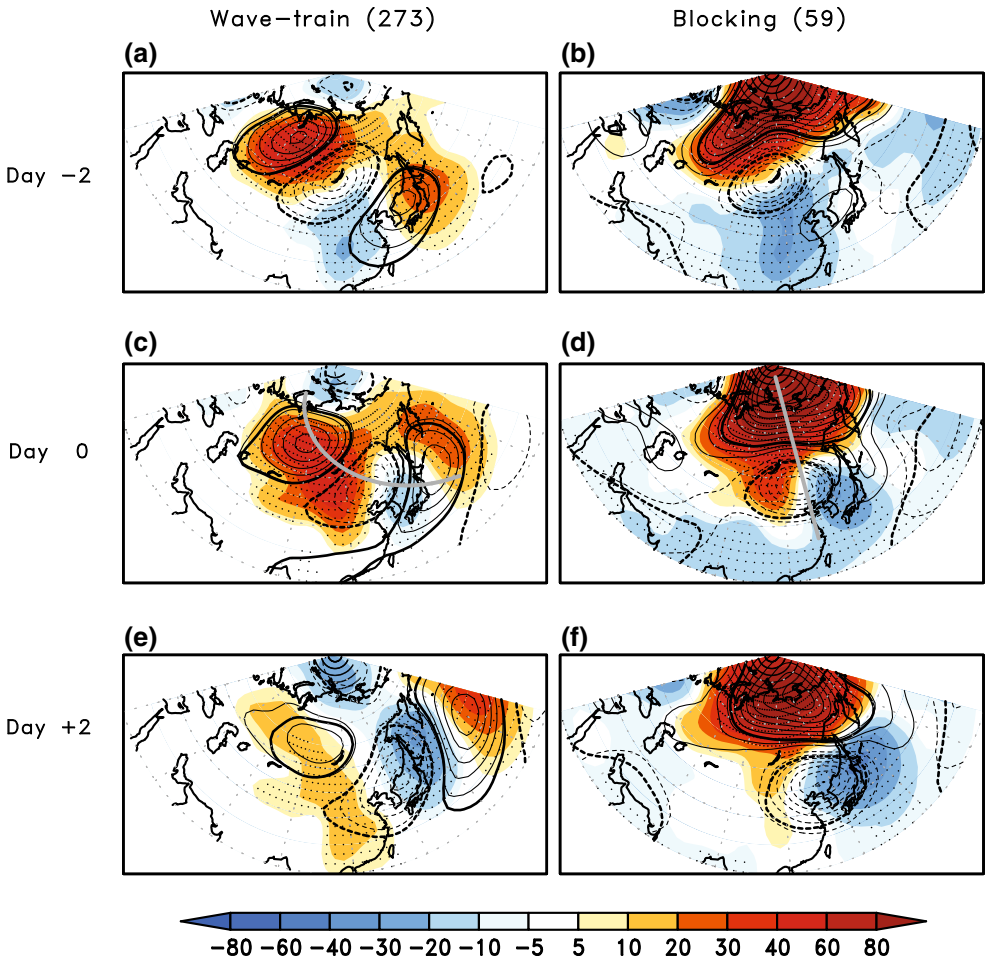

Fig. 3 Composite of Z anomalies at 300 hPa (contour; in intervals of 20 m, significant values at 95 % confidence level are represented by *thick lines*) and 850 hPa (*shaded*; significant values at 95 % confidence level are represented by *black dots*) for day −2 to day +2 relative to cold surge occurrences of **a**, **c**, **e** wave-train and **b**, **d**, **f** blocking types. *Grey thick lines* in **c**, **d** indicate the *wave-guided line* and the *blocking-ridge line*, respectively

Figure 3 shows the composite Z anomalies at 300 and 850 hPa that depict the lifecycle of the wave-train and the blocking cold surge from day −2 to day +2. The evolution from earlier times before day −2 will be discussed in later section. Note that, in the present study, the composite analysis is based on all 273 wave-train cases and all 59 blocking cases. For the wave-train type, 2 days prior to the occurrence of cold surge (day −2), a pronounced ridge-trough-ridge pattern is found over the Ural Mountains (50°E–90°E, 50°N–75°N), Lake Baikal (90°E–120°E, 45°N–65°N), and Korea-Japan (120°E–140°E, 30°N–45°N) (Fig. 3a). Over day −2 to day +2, this northwest-southeast-directed wave-train appears to propagate slowly toward southeast (Fig. 3a, c, e). In the lower troposphere (850 hPa), there is a southeastward progression of the anticyclone-cyclone couplet over Siberia and East Asia, where the anticyclone progresses from Siberia to southern China, linked to an expansion of the Siberian high toward East Asia. The Z anomalies also show a slight westward tilt with height for the wave-train case. In the case of blocking type, large positive and negative Z anomalies are found near the subarctic region and over East Asia, respectively (Fig. 3b, d, f). The positive anomalies of blocking are nearly barotropic (i.e., no vertical tilt) and appear stationary throughout the cold surge event, whereas the negative anomalies (i.e., troughs) show a baroclinic structure (i.e., westward tilt with height) and propagate slowly southeastward from Lake Baikal to Korea-Japan. The accompanied southward expansion of the Siberian High can be clearly seen in Fig. 3d. The expanded Siberian High forms a zonally-oriented anticyclone-cyclone couplet that induces intense cold advection over Korea and Japan. Note that the above results are based on statistically significant height anomalies at 95 % confidence level.

To further delineate processes responsible for the development of the two types of cold surges, in Fig. 4, we show the vertical cross-sections of the composite anomalies of Z and T along the lines of the wave-train and the

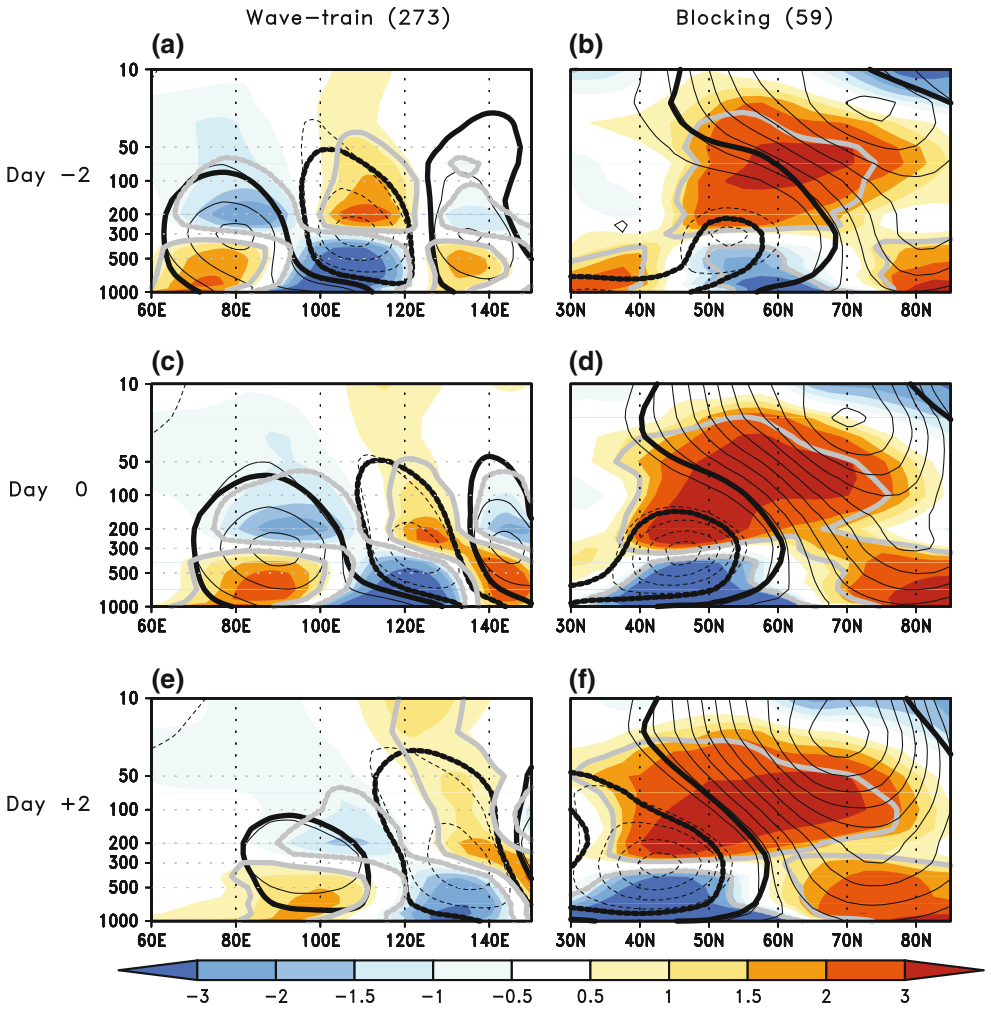

Fig. 4 *Vertical* cross-sections of Z anomalies (contour; in intervals of 30 m, significant values at 95 % confidence level are represented by *black thick lines*) and T anomalies (*shaded*; unit is K. Significant values at 95 % confidence level are represented by *grey thick lines*) along *grey thick lines* in Fig. 3c (from 60°E and 75°N to 150°E and 35°N) and 3d (meridional cross sections of longitude 120°E), for day −2 to day +2 relative to cold surge occurrences of **a**, **c**, **e** wave-train and **b**, **d**, **f** blocking types

blocking-ridge shown in Fig. 3c, d. For the wave-train type, troughs and ridges exhibit pronounced westward tilt with height below 100 hPa while warm and cold cores tilt eastward with height (Fig. 4a, c, e). The westward tilted trough-ridge and its corresponding eastward tilted cooling-warming structure characterizes the baroclinic growth of an extratropical synoptic-scale disturbance. By day +2, the Z anomalies over Lake Baikal (around 90°E–110°E) have weakened and now turned into an equivalent barotropic structure (Fig. 4e). In the blocking type of cold surge, the positive Z anomalies associated with the subarctic blocking (north of 50°N) are found for both of stratosphere and troposphere, while the negative Z anomalies of the mid-latitude trough (south of 50°N) range from the troposphere to the lower stratosphere (Fig. 4d–f). Maximum and minimum Z anomalies of the blocking and the trough are found at approximately 20 hPa (i.e., mid-stratosphere) and 300 hPa (i.e., tropopause), respectively. During the period from day −2 to day +2, the stratospheric ridge strengthens and extends downward and southward into the troposphere while the tropospheric trough intensifies locally and slowly progresses southward to East Asia finally inducing a cold surge over this region (Fig. 4b, d, f). In Fig. 4c, d, the low-level ridges (i.e., around 120°E in Fig. 4c and 50°N in Fig. 4d) migrate below the tropospheric cold anomalies, indicating the relationship between an amplification of the Siberian High and near-surface cold anomalies (we will revisit this point in Fig. 5).

Figure 5 presents near-surface features of the two types of cold surge including SLP, wind/temperature anomalies, and temperature advection at 850 hPa. Both types of cold surge are clearly linked to amplification of the Siberian High and its expansion toward East Asia (Fig. 5a–d). It indicates that for both types the amplification of the

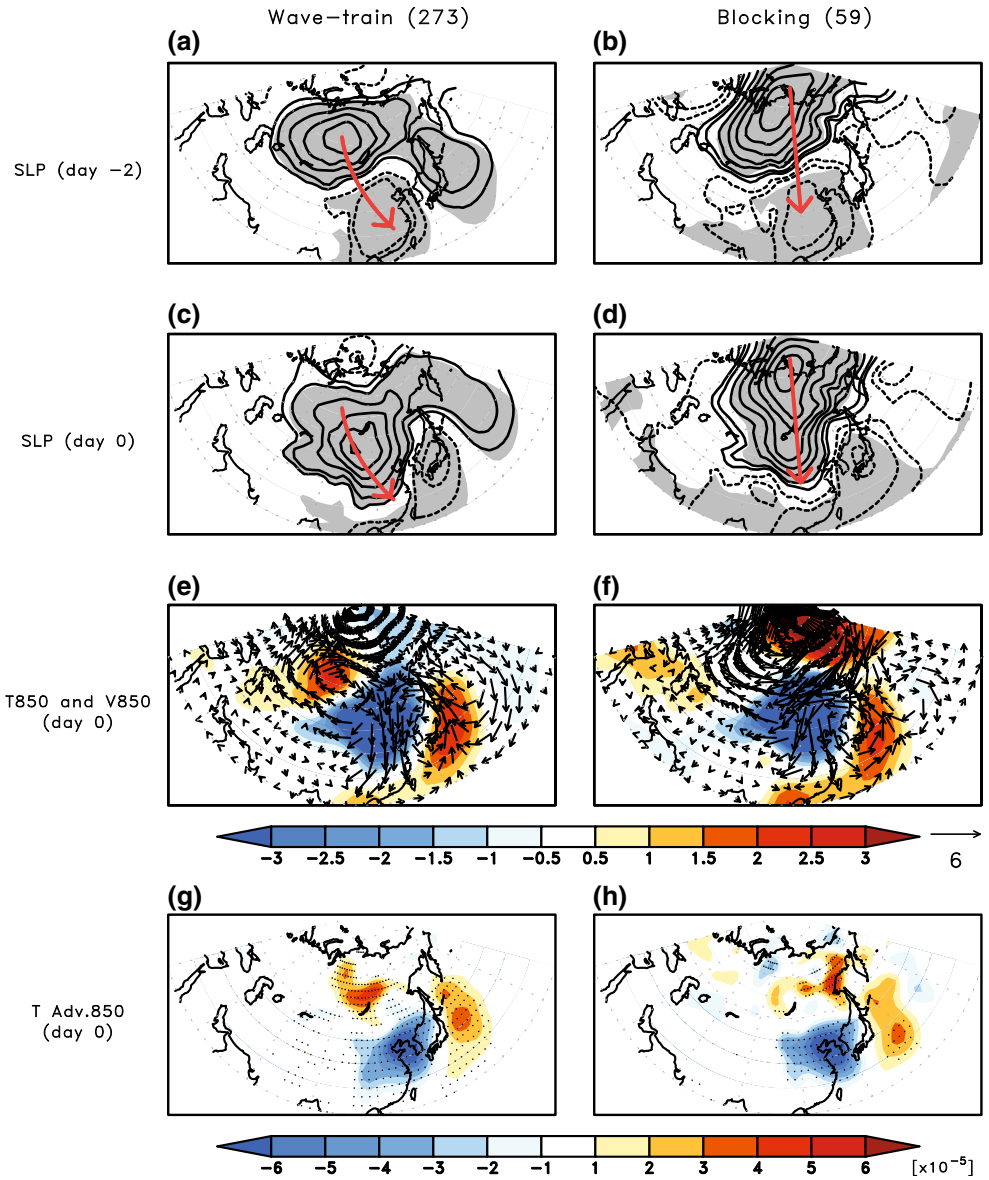

Fig. 5 Composite of SLP anomalies (contour; in intervals of 200 Pa, significant values at 95 % confidence level are *shaded*) for **a**, **b** day −2 and **c**, **d** day 0 relative to cold surge occurrences, **e**, **f** T anomalies (*shaded*) and wind anomalies (*vectors*), and **g**, **h** temperature advection (*shaded*; the unit is $\times 10^{-5}$ K s^{-1}, significant values at 95 % confidence level are represented by *black dots*) at 850 hPa for day 0 of **a**, **c**, **e**, **g** wave-train and **b**, **d**, **f**, **h** blocking types. *Red arrows* indicate the expansion of the Siberian High

Siberian High and its expansion toward East Asia reinforce local anomalous cold temperature. However the expansion of the high in the wave-train case originates from the interior of the Eurasian continent and is along a northwest-southeast direction (Fig. 5a, c). On the other hand, the expansion in the blocking case is along a southward direction with the center of the high stretching from the Arctic region to East Asia (Fig. 5b, d). A weak low pressure anomaly is present over Korea-Japan in both types of cold surge. We view the weak low pressure anomaly as an "auxiliary component" of the surge development, compared with the "primary component" (i.e., a strong Siberian High). However, this weak low pressure anomaly is also an important component to contribute to cold advection associated with the surge development. The development of the strong pressure gradient between the low-level high/low pressures is responsible for strong low-level cold advection across the temperature gradient (Fig. 5g, h) and the resulting abrupt temperature drop in East Asia (Fig. 5e, f). Specifically, in the wave-train case (Fig. 5e) the confluence of the lower-level flow associated with the southeastward expansion of the Siberian High and the deepening low over Korea-Japan provides anomalous northerly winds that bring Arctic air to East Asia. The cold

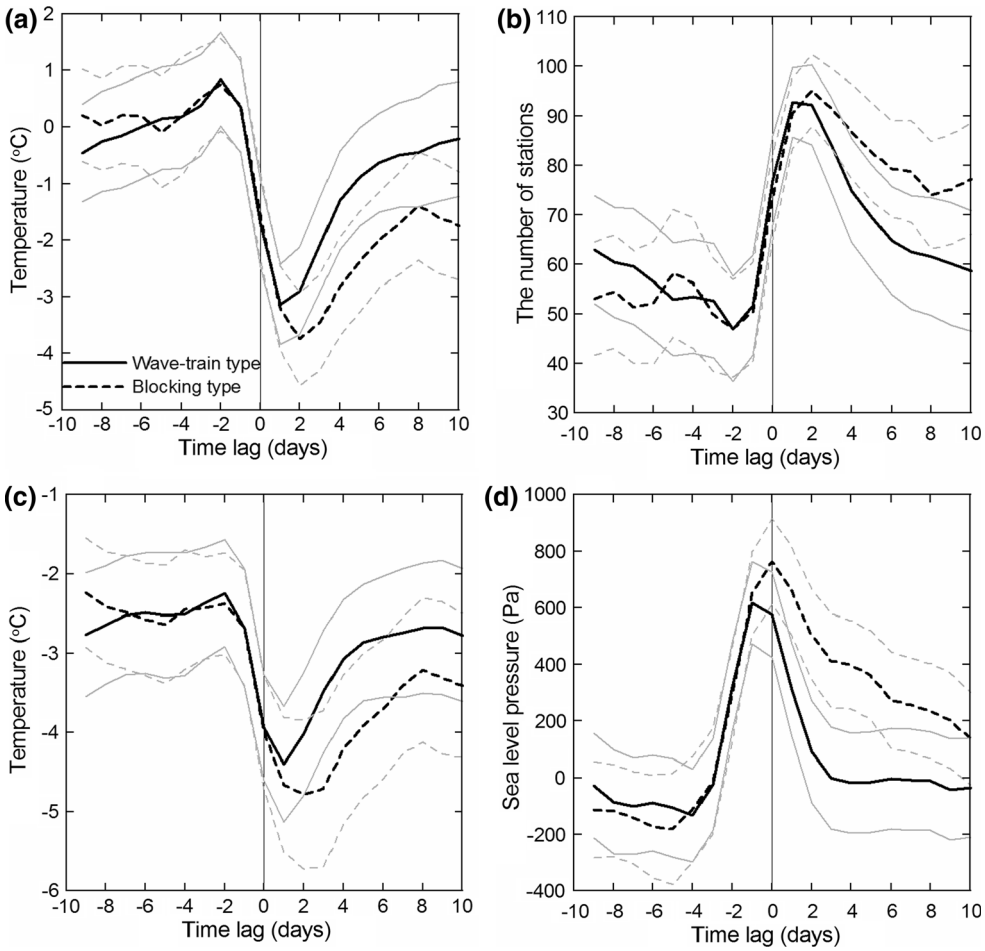

Fig. 6 The daily lag composites of **a** SAT anomalies averaged at all stations, **b** the number of stations which have negative SAT anomalies, **c** SAT anomalies averaged at stations detected in (**b**). The number of stations used in (**c**) differs before and after the onset of cold surges. **d** SLP anomalies averaged over 90°E–130°E and 40°N–65°N for cold surges of wave-train and blocking types. *Grey thin lines* indicate values of $\pm 1\ \sigma$ (standard deviation among cases for each type) errors relative to mean values

advection in the blocking case (Fig. 5f), on the other hand, is driven mainly by northeasterly winds along flows between the southward expansion of the Siberian High and the low (Fig. 5d). Contrasting Fig. 5c, d with Fig. 5e, f, the low-level anticyclonic (cyclonic) flows are associated with the cold (warm) anomalies. The low-level cold anomalies act to induce anticyclonic flow aloft and amplify the Siberian High (Takaya and Nakamura 2005a). The distribution of the 850-hPa temperature anomaly in the wave-train case is consistent with a developing baroclinic disturbance where warm (cold) anomalies are situated under upper level ridge (trough) (Fig. 3c, e). In the blocking type, besides dominant cold anomalies over East Asia, major warm anomalies appear in the subarctic region of the North Pacific and to the east of Japan. The latter seems to be driven by the warm advection found on the eastern portion of the surface low. Figure 5 also indicates that the blocking type cold surge tends to be typically more intense (in terms of the associated thermal advection) and cover a larger geographic domain compared to the wave-train type.

Figure 6a shows the composite SAT anomalies averaged over the entire East Asian region (90°E–130°E and 40°N–65°N) before and after the cold surge occurrence. Based on the SAT changes from day −1 to day +1, the wave-train type leads to a SAT-drop of ∼3 °C (from 0 to −3 °C) while the corresponding drop in the blocking type is ∼4 °C. It suggests that for the SAT averaged over the entire East Asia, the blocking type induce the larger SAT drop than the wave-train type. The larger drop for blocking can be due to a smaller number of cases (59 vs. 273). Thus, the SAT drops from day −1 to day +1 for the top 10 and the bottom 10 of typical cases are computed. The top 10 values are −6.92 °C and −7.56 °C for wave-train and blocking cases, respectively. The bottom 10 values are −0.68 and −2.25 °C. It helps the results that the blocking type brings larger SAT drop. Because the SAT drops are the values for the whole stations, note that the drops can be less than the values used in the cold surge definition. However, because it is the result from the SAT changes averaged over the just "entire" East Asian region, the result does not imply that the blocking type leads to more intense impact over broader regions compared with the wave-train type. Thus, we further present in Fig. 6b, c, respectively, the number of stations that have negative SAT anomalies and the corresponding average of the negative anomalies. During the wave-train and blocking type of cold

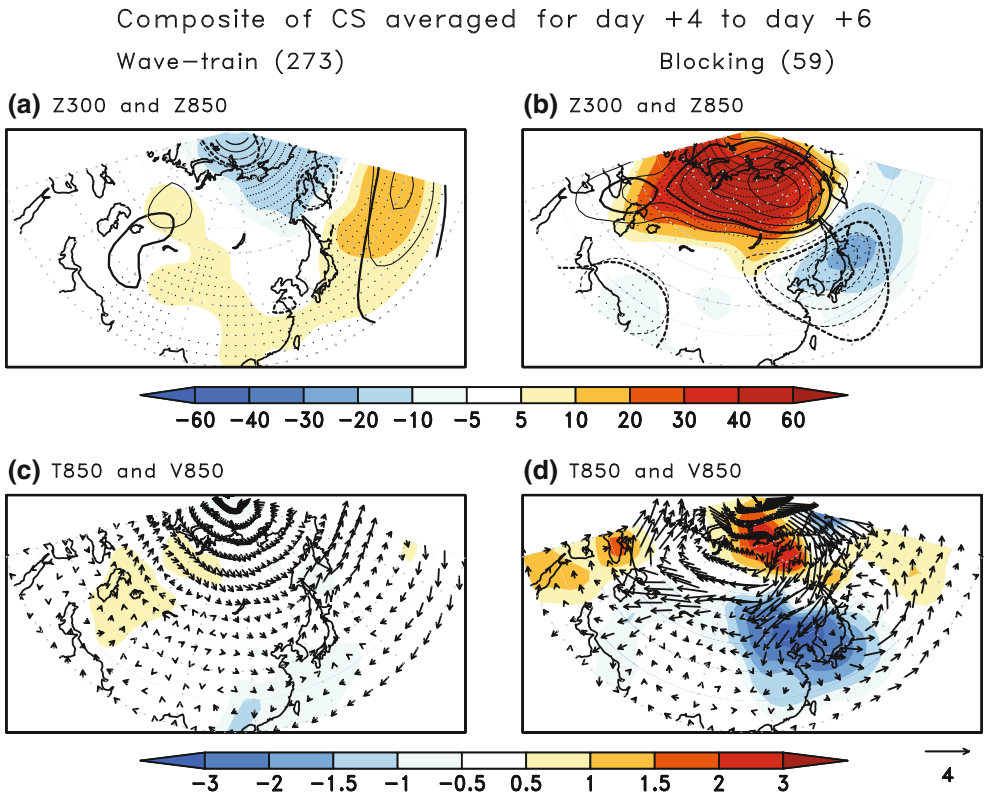

Fig. 7 Composite of Z anomalies at (**a**, **b**) 300 hPa (contour; in intervals of 20 m, significant values at 95 % confidence level are represented by *thick lines*) and 850 hPa (*shaded*; significant values at 95 % confidence level are represented by *black dots*), **c**, **d** T anomalies (*shaded*; unit is K) and wind anomalies (*vectors*) at 850 hPa averaged for day +4 to day +6 relative to of cold surge occurrences of **a**, **c** wave-train and **b**, **d** blocking types

surge, on average there are about 90 and 95 stations experiencing below-normal temperatures, respectively. The temperature drop averaged over these stations is also larger in the blocking type compared to that in the wave-train type. Results in Fig. 6a–c thus suggest that blocking type cold surge generally has higher intensity and affects a broader area. The differences in the intensity and the size of area influenced between the two types of cold surge are tied to the change of the Siberian High, as demonstrated in Fig. 6d. In both cases, the Siberian High starts a quick amplification from day −4. However, the amplification in the blocking type lasts until day 0 while the amplification in the wave-train case starts to cease on day −1. For the wave-train case, the Siberian High starts to weaken on day −1 and the rate of weakening is high. On the other hand, the amplification of the Siberian High associated with the blocking type continues till day 0 and then the Siberian High weakens slowly. The extra 1 day of sustained amplification can provide one among several reasons for the slow decaying of the Siberian High, inducing a strong and longer-lasting Siberian High during the blocking type cold surge. This subsequently leads to, in the wave-train case, a much shorter time (3–4 days versus more than 10 days) that the Siberian High takes to return to its climatological strength. The longer duration of the Siberian High for the blocking type is associated with the long-lasting blocking cold surge as shown in Fig. 6a–c. The atmospheric blocking is generally characterized by the large amplitude equivalent barotropic anticyclone which corresponds to a quasi-stationary state of the large-scale atmospheric circulation persisting over one or several weeks (Rex 1950). Thus, given the long duration of the atmospheric blocking, the blocking cold surge cannot easily return the status before the cold surge occurrence and the properties of the cold surges remain for the longer time.

As shown in Fig. 7, the difference in the duration of the two types of cold surge can also be demonstrated by the composite of Z anomalies (at 300 and 850 hPa) and temperature/wind anomalies (at 850 hPa) after the occurrence of the cold surge (e.g., averaged from day +4 to day +6). For the wave-train cold surge, there are no apparent features in these fields mimicking the wave-train seen in Fig. 3a, c, e. On the other hand, the dipole structure (Fig. 3b, d, f) characteristic of a blocking cold surge remains visible nearly a week after the surge. Figure 7c shows that central-northern China, Korea, and Japan are no longer under the influence of cold surge 4–6 days after a

wave-train event largely due to the diminishing cold advection. However, 4–6 days after a blocking event, below-normal temperatures that are sustained by cold advection associated with strong northeasterly winds are still found over East Asia (Fig. 7d).

4 Dynamical signals prior to wave-train and blocking cold surge

Identification of distinct circulation anomalies prior to the development of cold surge is of particular importance for understanding the origin and improving the prediction of cold surges. Here we explore dynamical features that emerge more than 1 week before the occurrence of the surge.

To depict the development of the stationary wave characteristic of the wave-train type cold surge, we calculate the stationary wave activity flux F_s introduced by Plumb (1985),

$$F_s = p\cos\phi \begin{pmatrix} v'^2 - \dfrac{1}{2\Omega\sin 2\phi}\dfrac{\partial(v'\Phi')}{\partial\lambda} \\ -u'v' + \dfrac{1}{2\Omega a\sin 2\phi}\dfrac{\partial(u'\Phi')}{\partial\lambda} \\ \dfrac{2\Omega\sin\phi}{S}\left[v'T' - \dfrac{1}{2\Omega a\sin 2\phi}\dfrac{\partial}{\partial\lambda}(T'\Phi')\right] \end{pmatrix}, \quad (4)$$

where the prime denotes the departure from zonal mean; p is pressure and (ϕ, λ) are the latitude and longitude, respectively; (u, v) represents respectively zonal and meridional winds; Φ is geopotential height; T is temperature; Ω and a are the Earth's rotation rate and mean radius, respectively; S is the static stability defined as

$$S = \frac{\partial\hat{T}}{\partial z} + \frac{\kappa\hat{T}}{H}, \quad (5)$$

where the caret indicates the area average over the northern hemisphere, k (= 287 J K^{-1} kg^{-1}/1,004 J K^{-1} kg^{-1}) is the ratio of gas constant to specific heat at constant pressure, and H (=8,000 m) is the constant scale height.

Figure 8 shows the time evolution of the composite of 300-hPa Z anomalies and the corresponding horizontal component of the wave activity flux from day −14 to day −4 for the wave-train type. Though there are no apparent signals on day −14 (Fig. 8a), a negative height perturbation appears southeast of Greenland on day −12 (Fig. 8b). The perturbation gets stronger during the period of day −12 to day −4 but remains nearly "stationary" (Fig. 8b–f). The dispersion of energy downstream, however, induces a positive Z anomaly over western Russia on day −10 (Fig. 8c) followed by a negative Z anomaly over the Lake Baikal on day −8 (Fig. 8d). The downstream propagation of wave activity is well captured by the anomalous stationary wave activity flux (arrows in Fig. 8 (Plumb 1985)), which spans across the wave-train and points toward East Asia where a cold surge occurs several days later. Note that in Fig. 8c, d, positive and negative Z perturbations over the North Pacific and the northwestern coast of North America, respectively, are found prior to the cold surge occurrence and the perturbations seem to lead to the wave-train started from the North Atlantic (Fig. 8e, f). It can indicate that the wave-train cold surges might originate in the North Pacific. However, there are no perturbations over the North America which can connect the perturbations over the North Pacific with the wave-train over the North Atlantic. Thus, the positive Z perturbation over Greenland and the wave-train across the Eurasia Continent might be produced by not the perturbations over the North Pacific but the downward stratospheric forcing (we will visit this point in the following paragraph.). In summary, the composite analysis suggests that the wave-train responsible for the occurrence of cold surges originates with a negative upper-tropospheric Z perturbation over the North Atlantic before cold surges.

A stratospheric PV anomaly tends to induce tropospheric dynamical adjustment processes that create anomalies in dynamical fields at the tropopause (Hartley et al. 1998; Ambaum and Hoskins 2002; Jeong et al. 2006). As discussed in Hoskins et al. (1985), isentropic surface tends to bend toward isolated positive IPV anomalies in stratosphere and the subsequent tropospheric adjustment can lead to the negative Z perturbation at tropopause. In light of this IPV-Z relationship, to trace the origin of this negative Z perturbation at 300 hPa around southeast of Greenland on day −12, we analyzed the IPV anomalies related to the wave-train cold surge. Figure 9 shows maps of composite IPV anomalies at 330 and 350 K (representing respectively upper troposphere and lower stratosphere) for the period day −14 to day −8. On day −14, a positive IPV anomaly at 350 K is found over the North Atlantic southeast of Greenland and there are no visible features at 330 K level (Fig. 9a, b). Two days later, a positive IPV anomaly appears southeast of Greenland at 330 K and geostrophic adjustment between the IPV and the Z anomalies around tropopause (i.e., isobaric level of 300 hPa or isentropic level of 330 K) occurs. This indicates that the negative Z perturbation may be associated with downward propagation of a positive IPV anomaly from lower stratosphere to tropopause, that is, it may incite the negative Z disturbances at tropopause. This downward propagation is also shown in the time-θ cross section of the IPV anomalies averaged over 40°W–10°E and 45°N–65°N (Fig. 9i, the region is marked with blue solid lines in Fig. 9a–h). The lower stratospheric positive IPV anomalies are observed

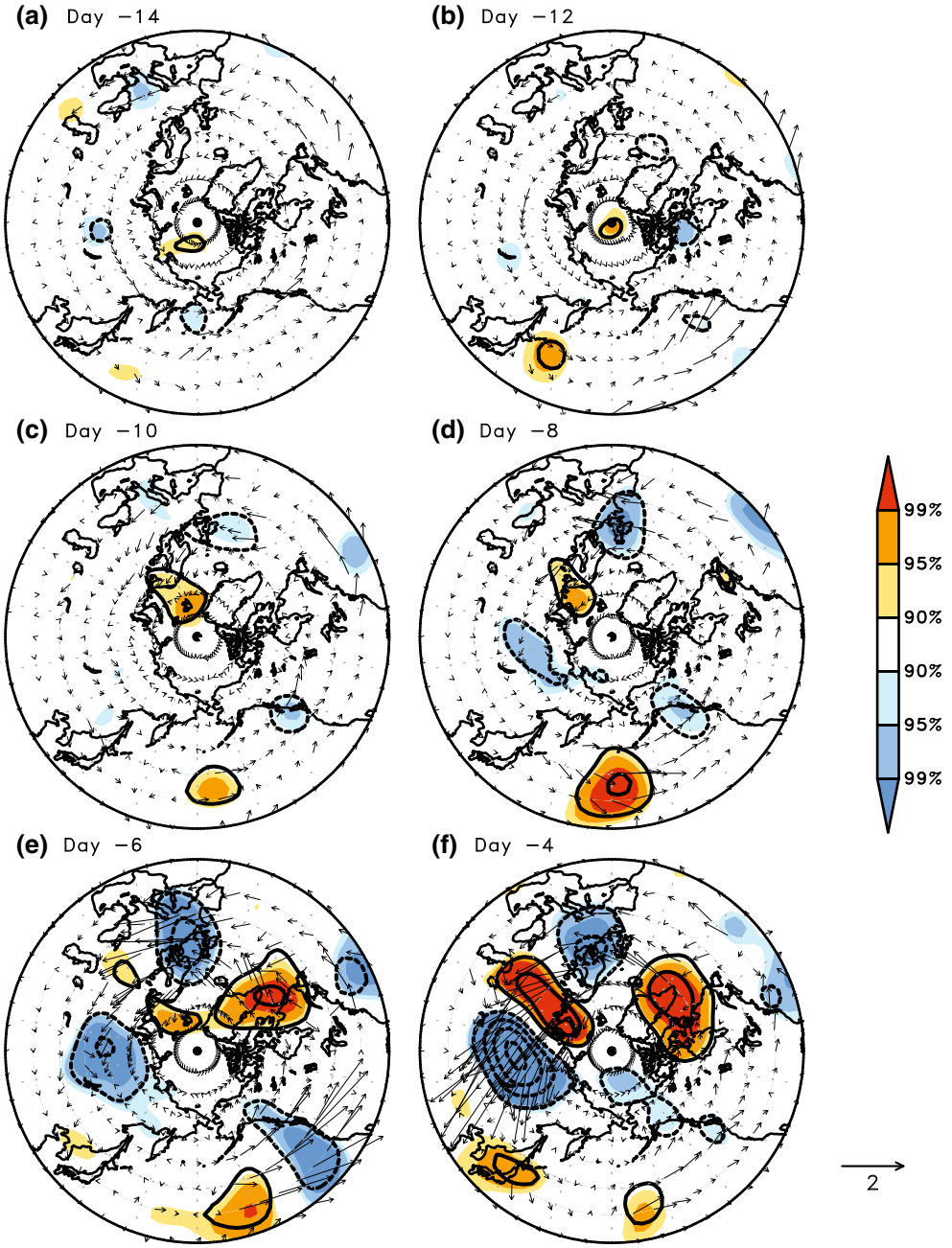

Fig. 8 Composite of Z anomalies (contour; in intervals of 20 m, significant values at 90, 95, and 99 % confidence level are *shaded*) and horizontal component anomalies of Plumb's wave activity flux (*vector*; unit is m^2/s^2) at 300 hPa for day −14 to day −4 relative to cold surge occurrences of wave-train type

ahead of ones at tropopause and the anomalies seem to propagate downward across 2 PVU line, referred as the dynamical tropopause (Hoskins and Berrisford 1988; Hoskins 1997). In particular, the feature has an influence on near-surface passing through the dynamical tropopause and troposphere (the significant values represented as red dots in Fig. 9i). Thus, the above processes related to positive IPV anomalies seem to provide the initial perturbation of negative Z anomalies leading to the wave-train disturbances.

As shown in Fig. 4b, d, f, cold surge of the blocking type is tied to positive Z anomalies of the high-latitudes in the mid-stratosphere centered at 20 hPa. To further investigate the stratospheric features prior to the cold surge, a time evolution of the Z anomalies at 20 hPa for the period from day −7 to day −1 are analyzed (Fig. 10). On day −7, the positive Z anomalies around the Arctic appear but are not significant (Fig. 10a). Figure 10b–d show that the increasing Z anomaly over the Arctic region grows stronger and slowly extends westward toward the northeastern

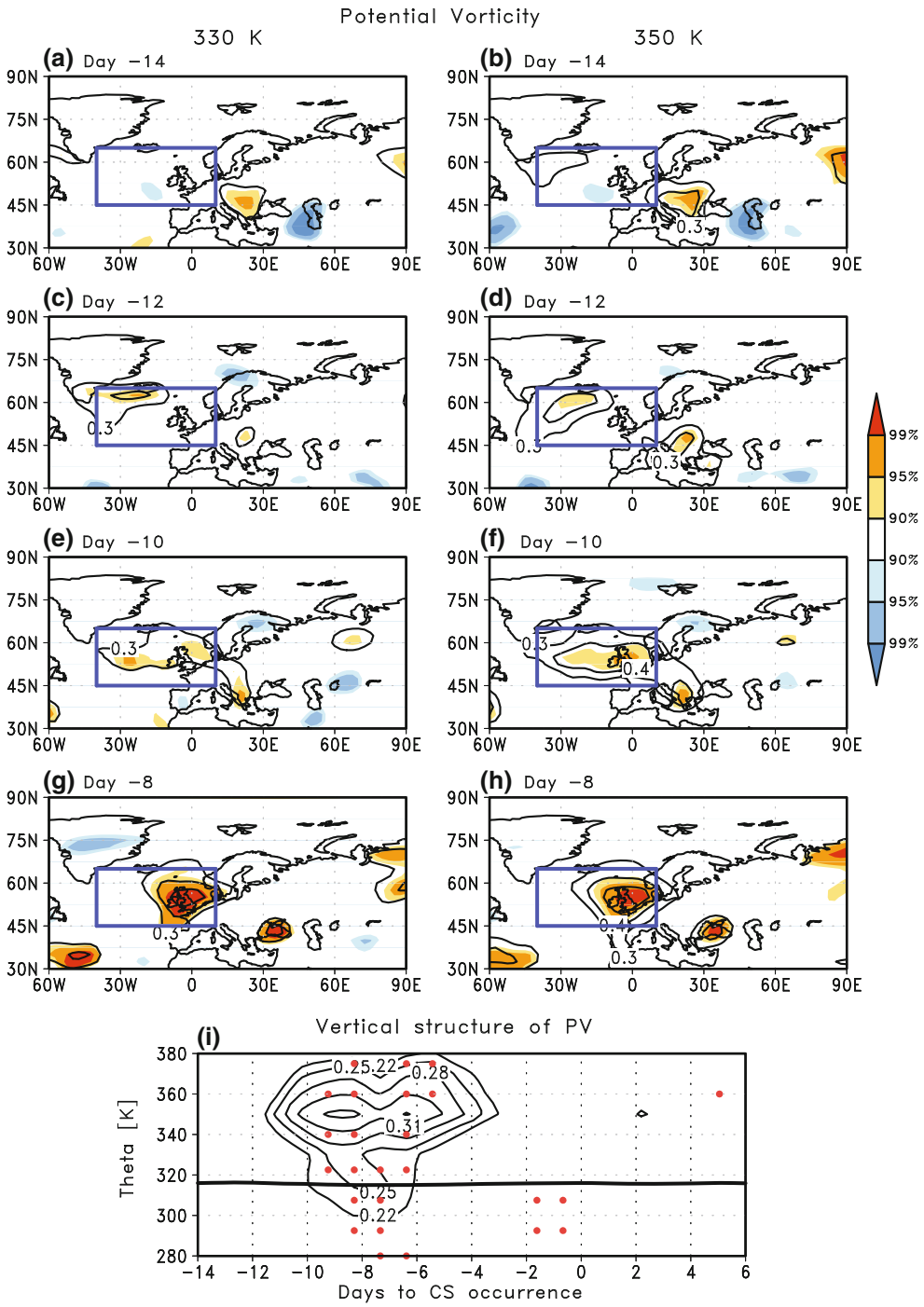

Fig. 9 **a–h** Composite of IPV anomalies (contoured every 0.1 PVU from 0.3 PVU, significant values at 90, 95, and 99 % confidence level are *shaded*) at 330 and 350°K for day −14 to day −8 relative to wave-train type cold surge occurrences. **i** *Vertical* structure of composite IPV anomalies (contoured every 0.03 PVU from 0.22 PVU, significant values at 95 % confidence level are represented as *red dots*) averaged over the *boxed* region in **a–h** (40°W–10°E, 45°N–65°N) during day −14 to day +6 relative to cold surge occurrences of the wave-train type. *Black thick line* indicates the 2 PVU, referred as the dynamical tropopause

Eurasia. On day −1, the positive Z anomalies in the stratosphere cover over the Arctic and the northern Eurasia. It indicates the amplification of a wave ½ ridge over Eurasia, which slowly retrogresses westward into the northeastern Eurasia prior to the cold surge occurrence. At the same time, two developments of the negative Z anomalies are found over the northern North America and the Western Europe, respectively, though the latter is much weaker than the former. The Z anomalies show a hemisphere-wide disturbance of the polar vortex during the days

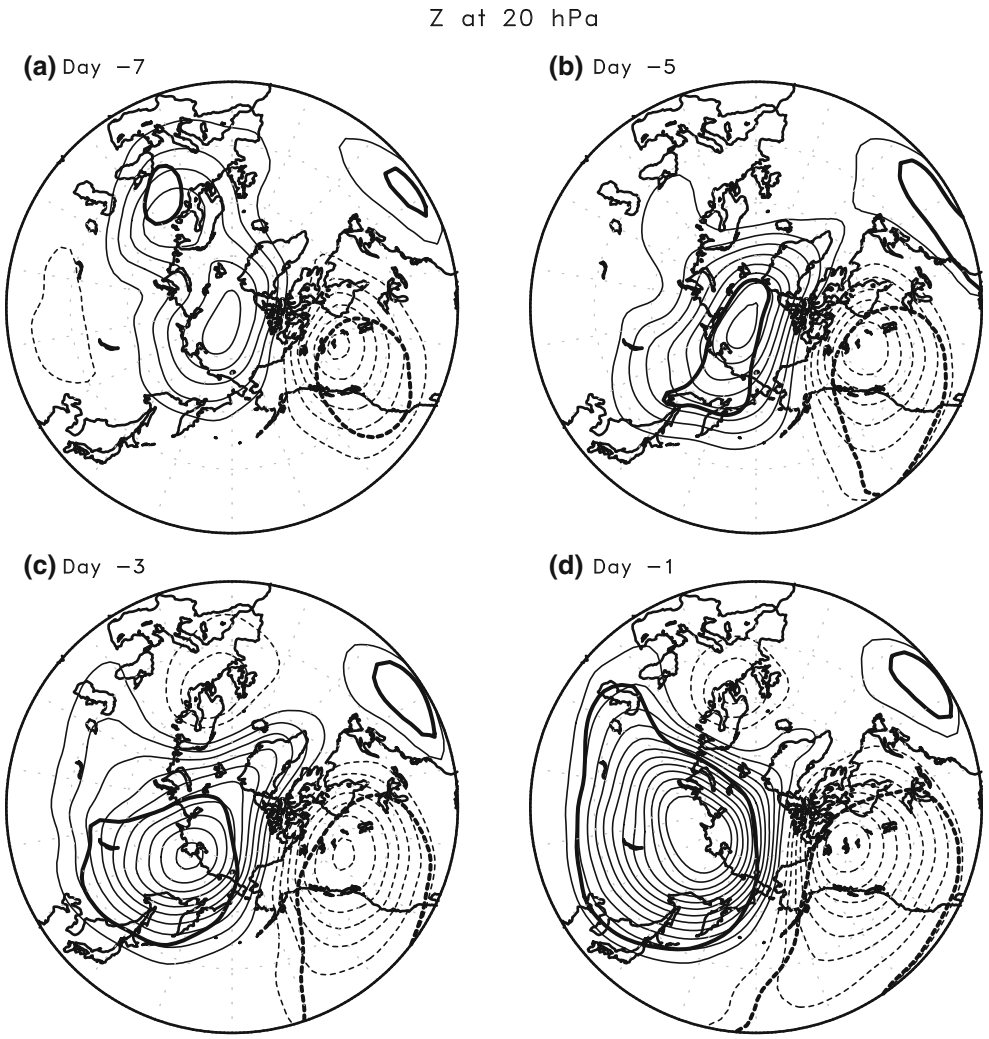

Fig. 10 Composite of Z anomalies at 20 hPa (contour; in intervals of 20 m, significant values at 95 % confidence level are represented by *thick lines*) for day −7 to day −1 relative to the blocking cold-surge occurrences

prior to the cold surge. These features are similar to the AO signatures presented in Baldwin and Dunkerton (1999) which discusses the effect of the complete breakdown of the stratospheric polar vortex on the tropospheric circulation. The similarities between the signal related to the blocking type cold surge and the AO signature in Baldwin and Dunkerton (1999) are the strong positive Z anomalies in the stratosphere around the Arctic and two sub-arctic negative Z anomalies. On the other hand, we do recognize that while the Z anomalies related to the AO is clearly zonally symmetric, the blocking-related signal shows the apparent dipole features of positive Z anomalies covering the Arctic and the northern Eurasia and negative Z anomalies over the northern North America with the weak low pressure over the Western Europe. We will revisit the relationship between the blocking type cold surge and the negative AO later.

Jeong et al. (2006) suggested that the rising of Z and the negative PV anomalies are found over the high-latitude regions in the stratosphere for 1 week prior to cold surge occurrence. Also, its corresponding positive potential temperature (θ) anomalies are located below the negative PV anomalies. To further clarify this, we plot composite anomalies of PV at 20 hPa and θ at 50 hPa for the period from day −7 to day −1 (Fig. 11a–d). Note that in Fig. 4b, d, f, the Z anomalies are centered at 20 hPa, while a center of θ anomalies is found at the 50 hPa. Compared to the Z anomalies shown in Fig. 10, the PV anomalies are localized. The localized PV anomalies are connected with the Z anomalies of a nonlocal feature. In Fig. 11a, b, negative PV anomalies reside over the Arctic region for 1 week prior to the occurrence of the blocking cold surge. Stratospheric warming and cooling are found over the Eurasian continent and North America, respectively, and the negative PV is

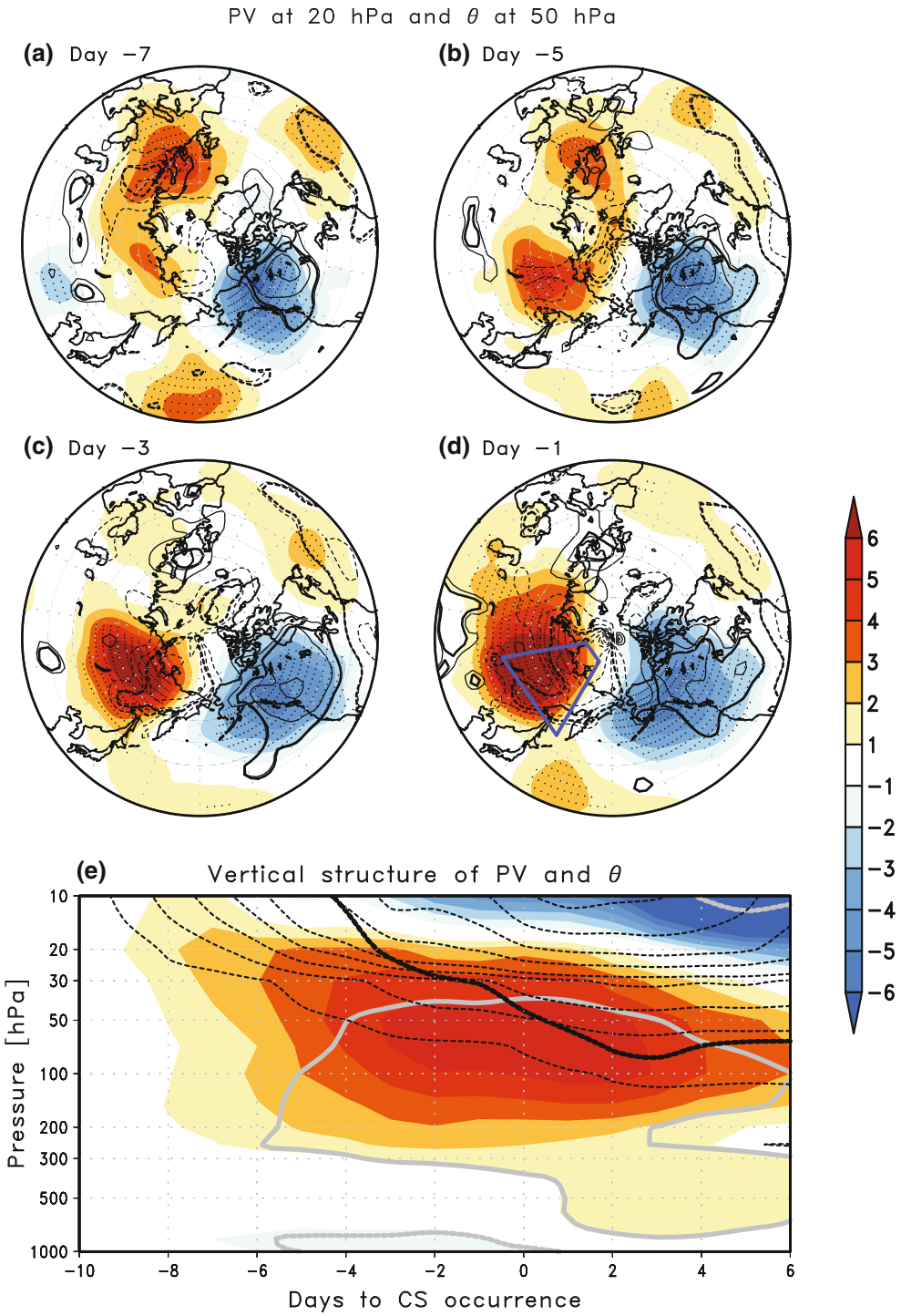

Fig. 11 **a–d** Composite of PV anomalies at 20 hPa (contour; in intervals of 5 PVU, significant values at 95 % confidence level are represented by *thick lines*) and θ anomalies at 50 hPa (*shaded*; significant values at 95 % confidence level are represented by *black dots*) for day −7 to day −1 relative to the blocking cold-surge occurrences. **e** *Vertical* cross section of composite PV anomalies (contour; in intervals of 2 PVU, significant values at 95 % confidence level are represented by *black thick lines*) and θ anomalies (*shaded*; unit is K, significant values at 95 % confidence level are represented by *grey thick lines*) averaged over the boxed region in **d** (100°E–150°E, 50°N–80°N) during day −10 to day +6 relative to cold surge occurrences of blocking type

located between the warming and cooling (Fig. 11c, d). The negative PV anomalies grow stronger. It seems to lead to the cold surge occurrence of the blocking type with the positive Z anomalies of the high-latitudes. Figure 11e shows the time evolution of the vertical structure of the composite PV and θ anomalies averaged over 100°E–

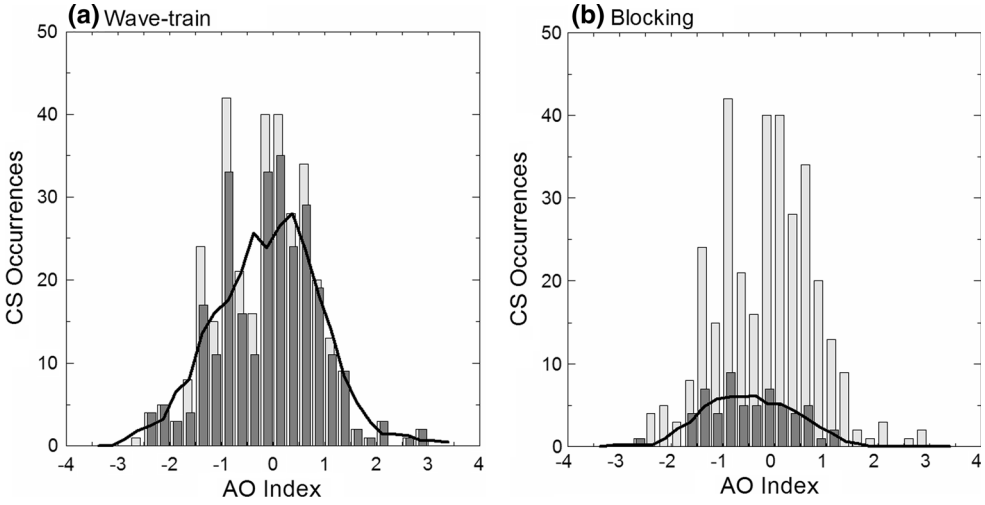

Fig. 12 The number of cold surge occurrences of **a** wave-train and **b** blocking types based on monthly AO index. *Light* and *dark bars* indicate cold surge occurrences of total and each type, respectively. *Thick line* is a sliding mean for 5-adjacent-band of *dark bar*

150°E and 50°N–80°N (defined by the box in Fig. 11d) where the amplification of PV anomaly and the stratospheric warming are most pronounced. It can be seen from Fig. 11e that approximately ten days before the cold surge occurrences, negative PV anomalies in the upper-stratosphere start to appear. Starting from day −10, the negative PV anomalies extend to the mid- and lower-stratosphere. At the same time, the corresponding strong warming centered on mid-stratosphere around 50 hPa seems to emerge to the lower-stratosphere. The stratospheric features are confined in the stratosphere above 200 hPa and do not directly reach the troposphere. Thus it acts on the stratospheric preconditions for the blocking type, suggesting that the cold surge of blocking type is also related to dynamical signal found in the stratosphere. The stratospheric negative PV signal and warming on modulating cold surge occurrences over East Asia are similar to those reported by Jeong et al. (2006), partly supporting our results of the stratospheric preconditions for the blocking type.

As abovementioned, a stratospheric Z and PV precondition prior the blocking cold surge (i.e., the stratospheric positive (negative) Z (PV) anomalies and their downward influence) resembles the process responsible for the stratospheric excitation of negative AO (Black 2002; Baldwin and Dunkerton 1999; Christiansen 2001). To delineate the relationship between blocking type cold surge and AO variability, we show in Fig. 12 the frequency distribution of cold surge occurrence of both types with respect to the AO index. The number of occurrences of the wave-train type is 137 and 136 for less and more than zero value of AO index, respectively. Also, the plotting the frequency of the wave-train type cold surge occurrences as a function of AO index reveals a nearly Gaussian distribution, indicating no preference for positive or negative AO. However, for blocking type, 42 cold surge occurrences are related to negative AO, while just 17 cold surges occur during positive AO. It indicates that the blocking type statistically shows a tendency to occur during the negative AO phase. In particular, no blocking cold surge is found when the AO index is greater than 1.25. That is, the AO-related polarity is evident only in the blocking type, a result consistent with findings by Park et al. (2011). This connection with AO can be interpreted in two ways: either a negative AO offers favorable flow conditions for the establishment of blocks or the AO is negative because a block is present. The former indicates that the negative AO can provide the stratospheric preconditions for the blocking type and further a good representation of AO variability and the initial state of the stratosphere in a model are critical for extended-range forecast of the blocking cold surge (Baldwin et al. 2003; Tang et al. 2007). The latter is thought to be the case for the North Atlantic Oscillation (NAO) pattern.

5 Summary and discussion

In this study, 332 cool-season cold surges over East Asia in the period 1954/1955–2005/2006 are classified into two types: the wave-train type and the blocking type. A synoptic and dynamical characterization is done for both types of cold surge. The 273 events belonging to the wave-train type is closely associated with a growing baroclinic disturbance manifesting itself as an upper-tropospheric wave-train. The wave-train type of cold surge is associated with the expansion of the Siberian High from interior of the Eurasia along a northwest-southeast direction with an intense cold advection driven by northerly winds. The 59 cold surges of the blocking type are characterized by a meridionally-oriented dipole in the upper-tropospheric Z anomalies, which consists of a subarctic blocking and the East Asian coastal trough. The southward expansion of the

Siberian High and the associated northeasterly winds sustain a strong cold advection over East Asia between the blocking and the coastal trough. Compared to the wave-train type, the blocking type brings colder temperatures and affects a broader area. The duration of the blocking-type cold surge is also considerably longer than that of the wave-train type. Therefore, although the wave-train cold surges occur much more frequently (273 vs. 59), the blocking cold surge tends to bring the most severe cold weather to East Asia.

The dynamical signals prior to both types of cold surge are also explored. A lower-stratospheric positive PV anomaly is found over the North Atlantic 2 weeks before the occurrence of the wave-train type cold surge. This PV anomaly seems to incite a negative Z anomaly around tropopause on southeast of Greenland approximately 12 days before the cold surge occurrence. As one of initial perturbations, this Z anomaly is associated with the development of a stationary wave-train across the Eurasian continent. Further baroclinic development downstream of this wave-train leads to generating the surge event. The development of the blocking type cold surge is preceded by the positive Z anomalies and the negative PV anomalies in the stratosphere over the Arctic region. The blocking related to the anomalies is growing stronger and slowly retrogressing westward from the Arctic to the northeastern Eurasia. The amplifying PV anomalies propagate downward into the mid- and lower-stratosphere, acting on stratospheric preconditions prior to the blocking type. This process bears some similarity with the stratospheric excitation of negative AO and indeed it is found that the blocking type cold surge tends to happen when AO is in its negative phase while the occurrence of wave-train cold surge does not have AO-phase preferences.

For cold surge of the blocking type, the present study suggests that the stratospheric circulation anomalies, which are characteristics of negative AO conditions, seem to lead the formation of the blocking high and the tropospheric cold air outbreak. Baldwin and Dunkerton (1999) showed the downward propagation of the AO signal from the stratosphere to the troposphere. This downward propagation of stratospheric anomalies and its effect on the high-latitudes cold air outbreaks via tropospheric AO was also simulated by Christiansen (2001). The results of our study are generally consistent with the idea of stratospheric modulation of tropospheric phenomena. However, from the opposite point of view, Martius et al. (2009) showed that the atmospheric blocking plays an important role in determining the anomalous stratospheric circulation events (e.g., sudden stratospheric warming events). That is, the blocking is not a response to the stratospheric circulation anomalies, but a precursor to them. These opposite views hint the possibility that the blocking prior to the occurrence of the cold surge influences the stratospheric circulation which in turn affects the blocking over East Asia. It would be interesting to investigate the interaction between blocking events and counterpart stratospheric circulation anomalies in more details in the future.

The stratospheric IPV anomalies found before the occurrence of the wave-train type cold surge are located over the North Atlantic near the exit region of the storm track (Chang et al. 2002). In addition, Campa and Wernli (2012) showed that IPV anomalies close to the tropopause over the North Atlantic can be modulated by the mid-latitude storms with a tropospheric origin. The high-latitude blocking in the North Pacific, associated with the blocking type cold surge, is also linked to breaking of synoptic-scale waves constituting the North Pacific storm track (Pelly and Hoskins 2003). Thus, storm track activities related to both of the North Atlantic and the North Pacific storm track seem to be connected with both types. An investigation of the connection between the cold surge occurrence and corresponding storm track variations will be our next step. The present study suggests that the wave-train and the blocking types are associated with the stratospheric modulation, that is, the downward propagation of stratospheric IPV and the preconditioning of stratospheric PV, respectively. For more comprehensive understanding and practical application, the downward influence of the stratospheric modulation can be dynamically validated by the piecewise potential vorticity inversion techniques (Davis 1992; Black 2002; Kim et al. 2009) and it will be our future work. In addition, the preference of blocking type cold surge to occur during the negative phase of AO suggests potential interaction between hemispheric-scale low-frequency variability and synoptic-scale cold surge. Previous studies have reported the impact of climate variability including AO, NAO and ENSO on the cold surge occurrences over East Asia (Jeong and Ho 2005; Park et al. 2011). Future research will also include efforts to understand how various modes of climate variability project into the statistics of the two types of cold surge.

Acknowledgments The daily-mean SAT at Chinese and Korean stations used in this study were provided by the China Meteorology Administration and the Korea Meteorology Administration. The Georgia Tech authors (Deng and Park) were supported by DOE Office of Science Regional and Global Climate Modeling (RGCM) program under Grant DE-SC0005596 and the NASA Energy and Water Cycle Study (NEWS) under grant NNX09AJ36G. The SNU author (Ho) was funded by the National Research Foundation of the Korean government (NRF 2009-0093458) and Korea Meteorological Administration Research and Development Program under Grant CATER 2012-2040. This research was supported by Basic Science Research Program through the NRF funded by the Ministry of Education, Science and Tech (NRF-2012R1A6A3A03038637). The study was performed during the first author's Ph.D. course at the SNU, Korea and finalized at the Georgia Tech.

References

Ambaum MHP, Hoskins BJ (2002) The NAO troposphere-stratosphere connection. J Clim 15(14):1969–1978

Baldwin MP, Dunkerton TJ (1999) Propagation of the Arctic Oscillation from the stratosphere to the troposphere. J Geophys Res-Atmos 104(D24):30937–30946

Baldwin MP, Stephenson DB, Thompson DWJ, Dunkerton TJ, Charlton AJ, O'Neill A (2003) Stratospheric memory and skill of extended-range weather forecasts. Science 301(5633):636–640

Black RX (2002) Stratospheric forcing of surface climate in the Arctic Oscillation. J Clim 15(3):268–277

Campa J, Wernli H (2012) A PV perspective on the vertical structure of mature midlatitude cyclones in the northern hemisphere. J Atmos Sci 69(2):725–740. doi:10.1175/Jas-D-11-050.1

Chang EKM, Lee SY, Swanson KL (2002) Storm track dynamics. J Clim 15(16):2163–2183

Chen TC (2002) A North Pacific short-wave train during the extreme phases of ENSO. J Clim 15(17):2359–2376

Chen TC, Yen MC, Huang WR, Gallus WA (2002) An East Asian cold surge: case study. Mon Weather Rev 130(9):2271–2290

Chen TC, Huang WR, Yoon J (2004) Interannual variation of the East Asian cold surge activity. J Clim 17(2):401–413

Christiansen B (2001) Downward propagation of zonal mean zonal wind anomalies from the stratosphere to the troposphere: model and reanalysis. J Geophys Res-Atmos 106(D21):27307–27322

Cohen J, Saito K, Entekhabi D (2001) The role of the Siberian high in Northern Hemisphere climate variability. Geophys Res Lett 28(2):299–302

Davis CA (1992) Piecewise potential vorticity inversion. J Atmos Sci 49(16):1397–1411

Ding Y, Krishnamurti TN (1987) Heat-budget of the Siberian high and the winter monsoon. Mon Weather Rev 115(10):2428–2449

Gong DY, Ho CH (2002) The Siberian high and climate change over middle to high latitude Asia. Theor Appl Climatol 72(1–2):1–9

Hartley DE, Villarin JT, Black RX, Davis CA (1998) A new perspective on the dynamical link between the stratosphere and troposphere. Nature 391(6666):471–474

Hoskins B (1997) A potential vorticity view of synoptic development. Meteorol Appl 4(4):325–334. doi:10.1017/s1350482797000716

Hoskins B, Berrisford P (1988) A potential vorticity perspective of the storm of 15–16 October 1987. Weather 43(3):122–129. doi:10.1002/j.1477-8696.1988.tb03890.x

Hoskins BJ, Mcintyre ME, Robertson AW (1985) On the use and significance of isentropic potential vorticity maps. Q J Roy Meteor Soc 111(470):877–946

Jeong J-H, Ho C-H (2005) Changes in occurrence of cold surges over East Asia in association with Arctic Oscillation. Geophys Res Lett 32:L14704. doi:10.1029/2005GL023024

Jeong J-H, Kim B-M, Ho C-H, Chen D, Lim G-H (2006) Stratospheric origin of cold surge occurrence in East Asia. Geophys Res Lett 33:L14710. doi:10.1029/2006GL026607

Jeong J-H, Kim B-M, Ho C-H, Noh Y-H (2008) Systematic variation in wintertime precipitation in East Asia by MJO-induced extratropical vertical motion. J Clim 21(4):788–801. doi:10.1175/2007jcli1801.1

Joung CH, Hitchman MH (1982) On the role of successive downstream development in East Asian Polar air outbreaks. Mon Weather Rev 110(9):1224–1237

Kalkstein LS, Tan GR, Skindlov JA (1987) An evaluation of 3 clustering procedures for use in synoptic climatological classification. J Clim Appl Meteorol 26(6):717–730

Kalnay E, Kanamitsu M, Kistler R, Collins W, Deaven D, Gandin L, Iredell M, Saha S, White G, Woollen J, Zhu Y, Chelliah M, Ebisuzaki W, Higgins W, Janowiak J, Mo KC, Ropelewski C, Wang J, Leetmaa A, Reynolds R, Jenne R, Joseph D (1996) The NCEP/NCAR 40-year reanalysis project. Bull Am Meteorol Soc 77(3):437–471

Kim B-M, Jeong J-H, Kim S-J (2009) Investigation of stratospheric precursor for the East Asian cold surge using the potential vorticity inversion technique. Asia-Pac J Atmos Sci 45(4):513–522

Lau NC, Lau KM (1984) The structure and energetics of midlatitude disturbances accompanying cold-air outbreaks over East-Asia. Mon Weather Rev 112(7):1309–1327

Lu FC, Juang HMH, Liao CC (2007) A numerical case study of the passage of a cold surge across Taiwan. Meteorol Atmos Phys 95:27–52. doi:10.1007/s00703-006-0192-9

Martius O, Polvani LM, Davies HC (2009) Blocking precursors to stratospheric sudden warming events. Geophys Res Lett 36:L14806. doi:10.1029/2009gl038776

Park T-W, Jeong J-H, Ho C-H, Kim S-J (2008) Characteristics of atmospheric circulation associated with cold surge occurrences in East Asia: a case study during 2005/06 winter. Adv Atmos Sci 25(5):791–804. doi:10.1007/s00376-008-0791-0

Park T-W, Ho C-H, Yang S, Jeong J-H (2010) Influences of Arctic Oscillation and Madden-Julian Oscillation on cold surges and heavy snowfalls over Korea: a case study for the winter of 2009–2010. J Geophys Res-Atmos 115:D23122. doi:10.1029/2010JD014794

Park T-W, Ho C-H, Yang S (2011) Relationship between the Arctic Oscillation and Cold Surges over East Asia. J Clim 24(1):68–83. doi:10.1175/2010jcli3529.1

Pelly JL, Hoskins BJ (2003) A new perspective on blocking. J Atmos Sci 60(5):743–755

Plumb RA (1985) On the three-dimensional propagation of stationary waves. J Atmos Sci 42(3):217–229

Rex DF (1950) Blocking action in the middle troposphere and its effect upon regional climate. Tellus 2(3):196–211. doi:10.1111/j.2153-3490.1950.tb00331.x

Takaya K, Nakamura H (2005a) Mechanisms of intraseasonal amplification of the cold Siberian high. J Atmos Sci 62(12):4423–4440

Takaya K, Nakamura H (2005b) Geographical dependence of upper-level blocking formation associated with intraseasonal amplification of the Siberian high. J Atmos Sci 62(12):4441–4449

Tang Y, Lin H, Derome J, Tippett MK (2007) A predictability measure applied to seasonal predictions of the Arctic Oscillation. J Clim 20(18):4733–4750. doi:10.1175/Jcli4276.1

Thompson DWJ, Wallace JM (1998) The Arctic Oscillation signature in the wintertime geopotential height and temperature fields. Geophys Res Lett 25(9):1297–1300

Yang S, Lau KM, Kim KM (2002) Variations of the East Asian jet stream and Asian-Pacific-American winter climate anomalies. J Clim 15(3):306–325

Zhang Y, Wang WC (1997) Model-simulated northern winter cyclone and anticyclone activity under a greenhouse warming scenario. J Clim 10(7):1616–1634

Zhang Y, Sperber KR, Boyle JS (1997) Climatology and interannual variation of the East Asian winter monsoon: results from the 1979–95 NCEP/NCAR reanalysis. Mon Weather Rev 125(10):2605–2619